ACS APPLIED MATERIALS & INTERFACES

Research Article

www.acsami.org

Delineating Fibronectin Bioadhesive Micropatterns by Photochemical Immobilization of Polystyrene and Poly(vinylpyrrolidone)

Olof Sterner,[†] Marta Giazzon,[‡] Stefan Zürcher,[†,§] Samuele Tosatti,[†,§] Martha Liley,[‡] and Nicholas D. Spencer*[,†]

[†]Laboratory for Surface Science and Technology, Department of Materials, ETH Zurich, Vladimir-Prelog-Weg 5, CH-8093, Zürich, Switzerland

[‡]Nanotechnology & Life Sciences, CSEM, Jaquet Droz 1, CH-2002 Neuchâtel, Switzerland

[§]SuSoS AG, Lagerstrasse 14, CH-8600 Dübendorf, Switzerland

Supporting Information

ABSTRACT: Bioadhesive micropatterns, capable of laterally confining cells to a 2D lattice, have proven effective in simulating the in vivo tissue environment. They reveal fundamental aspects of the role of adhesion in cell mechanics, proliferation, and differentiation. Here we present an approach based on photochemistry for the fabrication of synthetic polymer micropatterns. Perfluorophenyl azide (PFPA), upon deep-UV exposure, forms a reactive nitrene capable of covalently linking to a molecule that is in close proximity. PFPA has been grafted onto a backbone of poly(allyl amine), which readily forms a self-assembled monolayer on silicon wafers or glass. A film of polystyrene was applied by spin-coating, and by laterally confining the UV exposure through a chromium-on-quartz photomask, monolayers of polymers could be immobilized in circular microdomains. Poly(vinylpyrrolidone) (PVP) was attached to the background to form a barrier to nonspecific protein adsorption and cell adhesion. Micropatterns were characterized with high-lateral-resolution time-of-flight secondary ion mass spectrometry (TOF-SIMS), which confirmed the formation of polystyrene domains within a PVP background. Fluorescence−microscopy adsorption assays with rhodamine-labeled bovine serum albumin demonstrated the nonfouling efficiency of PVP and, combined with TOF-SIMS, allowed for a comprehensive characterization of the pattern geometry. The applicability of the micropatterned platform in single-cell assays was tested by culturing two cell types, WM 239 melanoma cells and SaOs-2 osteoblasts, on micropatterned glass, either with or without backfilling of the patterns with fibronectin. It was demonstrated that the platform was efficient in confining cells to the fibronectin-backfilled micropatterns for at least 48 h. PVP is thus proposed as a viable, highly stable alternative to poly(ethylene glycol) for nonfouling applications. Due to the versatility of the nitrene-insertion reaction, the platform could be extended to other polymer pairs or proteins and the surface chemistry adapted to specific applications.

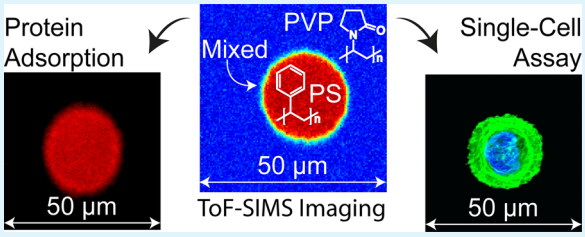

KEYWORDS: *micropatterning, bioadhesion, single-cell assay, photochemistry, perfluorophenyl azide, poly(vinylpyrrolidone)*

INTRODUCTION

Bioadhesive micropatterns, on which the positions of cells can be precisely controlled, have become an important tool in cell biology. The confinement that the cell experiences within the micropattern mimics the in vivo tissue environment, which imposes constraints on cell spreading, in contrast to traditional cell culture, where cells are free to adopt any shape.[1] On micropatterns, cells can further be forced to span across nonadhesive regions,[2,3] a frequently encountered in vivo scenario. As a consequence, cells confined to micropatterns have been reported to retain phenotype for longer durations compared to traditionally cultured cells.[4] By precise control over cell spreading and the number of cell−cell interactions, the cell-phenotype diversity can be minimized by ensuring that the extracellular environment is identical for all cells. In addition to enabling confinement, the pattern geometry itself has a profound effect on cell behavior and mechanics, guiding the distribution of stress fibers and focal adhesion[2,3,5] and the organization of intracellular compartments[6] and influencing differentiation,[7,8] mitotic-spindle position,[9] and cell migration.[10,11] Furthermore, maintaining cells in well-defined locations has the practical advantage of allowing single cells to be individually treated and afterward addressed on a 2D lattice for further experiments or analysis.

Micropatterns have typically been prepared by means of either soft lithography or photolithography, but maskless approaches have also been employed.[12,13] The formation of an inert background where cell spreading is inhibited is critical

Received: June 28, 2014
Accepted: September 25, 2014
Published: September 25, 2014

   dx.doi.org/10.1021/am5042093 | ACS Appl. Mater. Interfaces 2014, 6, 18683−18692

for bioadhesive-micropattern fabrication. To this end, a dense, hydrophilic polymer coating is typically prepared by grafting-to, grafting-from, or self-assembly methodologies.[14] The stability of the polymer coating can of course be increased by covalently tethering the polymer to the surface; however, the simplicity of self-assembly and its versatility in terms of substrate choice are some of the great advantages of physisorbed nonfouling coatings, such as poly(L-lysine) grafted with poly(ethylene glycol) (PLL-*g*-PEG).[15−17] PLL-*g*-PEG, in combination with photolithography, has been used to fabricate bioadhesive micropatterns by a variety of methods, including direct UV decomposition of the PEG functionality,[18] selective molecular assembly patterning (SMAP),[19] and molecular assembly patterning by lift-off (MAPL).[20] The drawbacks of the physisorbed PEG coating include mediocre stability under cell-culture conditions,[21,22] desorption of the cationic backbone in high-ionic-strength medium,[23] and, for long-term applications, the susceptibility of PEG to oxidative cleavage.[24,25] Recent data suggest, however, that PLL-*g*-PEG, self-assembled under high-temperature conditions, forms an ultradense PEG coating with superior long-term stability.[26]

Another approach to passivating surfaces is to photochemically immobilize a nonfouling polymer. In this regard, different photochemical moieties have been reported to be suitable for surface tethering of macromolecules, including benzophenone,[27] α-diazo esters,[28] and aryl azides.[29] In this approach the macromolecules are covalently attached to the photosensitive moiety through unselective insertion reactions, leading to monolayer coatings of random macromolecular conformation, in contrast to traditional grafting-to methodologies. Several hydrophilic macromolecules, immobilized by means of perfluorophenyl azide (PFPA) as the photochemical moiety, have been reported to render the surface nonfouling,[30−32] including PEG, dextran, and poly(2-ethyl-2-oxazoline). Further, PFPA has been linked to a cationic macromolecule, to form a graft-copolymer adhesion promoter, and surface-anchored electrostatically, as in the case of poly(allyl amine) grafted with PFPA (PAAm-*g*-PFPA).[30,33,34] This approach combines the flexibility of PLL-*g*-PEG, with regard to substrate choice, and the versatility of the phototriggered insertion reaction to immobilize virtually any organic molecule. We have previously reported that, despite the noncovalent substrate interaction, the nonfouling performance of such photochemically immobilized polymer coatings can be retained under high ionic strength conditions.[30,33] This was possibly due to cross-linking of PAAm-*g*-PFPA during azide decomposition to nitrene and increasing the number of amine−surface interactions per macromolecule. Photochemistry has been combined with photolithography to fabricate nano- and micropatterns;[35,36] however, few examples exist for the preparation of bioadhesive micropatterns.[32,37,38]

An alternative to PEG, which has gained increasing interest in recent years as a nonfouling polymer, is poly(vinylpyrrolidone) (PVP).[39] Due to its biocompatibility[40] and high solubility, both in water and various organic solvents, PVP has found numerous biomedical applications including contact lenses,[41] wound dressings,[42] pharmaceuticals,[43] and biomaterials.[44] In addition, PVP has been photochemically linked to polyurethane catheters functionalized with aryl azides, with a reported reduction of thrombogenicity in vitro.[45] Monolayer films of PVP are rarer but have recently been prepared using controlled radical polymerization techniques.[46] However, due to the unconjugated monomer, the propagating radical is not resonance-stabilized, which can lead to unwanted side reactions and high polydispersity.[47] The resulting monolayer films are stable and resist adsorption of a variety of proteins,[48] including full human serum.[30] Recently, PVP has also been demonstrated to resist cell adhesion.[49] The photochemical immobilization route, mentioned above, is attractive, as PVP is commercially available in molecular weights ranging from thousands to millions of daltons, and no postmodification of the polymer chain is necessary. Such photochemically prepared monolayer films have been previously prepared and were shown to resist adhesion of marine bacteria and algae spores.[30,33] We hypothesized that the outstanding biocompatibility and stability of PVP would make it an ideal choice as the inert background in a novel micropatterned platform for use in single-cell assays.

In the current study, we report on the fabrication of bioadhesive micropatterns consisting of polystyrene (PS) and poly(vinylpyrrolidone) (PVP). Spots of polystyrene were photochemically immobilized on a self-assembled monolayer of PAAm-*g*-PFPA by UV exposure through a chromium-on-quartz photomask. In a second step, PVP was photochemically attached in the previously nonilluminated areas, to form the nonadhesive background. The chemical composition of the micropatterns was characterized using high-lateral-resolution time-of-flight secondary ion mass spectrometry (TOF-SIMS), which confirmed the formation of chemically distinct microdomains. Adsorption of rhodamine-labeled bovine serum albumin corroborated the nonadhesive nature of the PVP. Two different cell types, melanoma and osteoblasts, were cultured on micropatterned glass to determine the applicability of the coating in single-cell assays. Prior to the assay, half of the samples were backfilled with fibronectin—an extracellular matrix protein carrying the Arg-Gly-Asp (RGD) peptide sequence—enabling integrin-mediated adhesion. In the case of fibronectin-backfilled samples, cells were found to adhere uniquely to the PS spots and were unable to spread onto the inert background, even after 48 h, demonstrating the stability of the coating in cell medium. Preincubation with fibronectin increased the attachment yield and prevented detachment during cell division, but it was not critical for adhesion per se. Due to the versatility of the photochemical method, the protocol can be extended to involve immobilization of other polymer pairs or proteins and consequently be fine-tuned to specific applications. Further, the possibility of generating ad hoc patterns is only limited by the capacity of controlling how the UV light is distributed on the surface.

MATERIALS AND METHODS

Standard Chemicals. The following ACS-grade solvents were used: toluene (Fluka), 2-propanol (Scharlau Chemie), ethanol (Scharlau Chemie), chloroform (Sigma-Aldrich), and ethyl acetate (Sigma-Aldrich). The following polymers were purchased from Sigma-Aldrich: poly(vinylpyrrolidone) (PVP, 1300 kDa), polystyrene (PS, 2000 kDa), and poly(allyl amine) hydrochloride (PAAm·HCl, 14 kDa). 4-[2-Hydroxyethyl]piperazine-1-[2-ethanesulfonic acid] (HEPES) buffer salt was acquired from Fluka Chemie, potassium carbonate (K_2CO_3) was from Merck, and perfluorophenyl azide *N*-hydroxysuccinimidyl ester (PFPA-NHS) and bovine serum albumin labeled with rhodamine isothiocyanate (BSA-TRITC) were obtained from SuSoS AG. Components of cell culture medium were McCoy's 5A, fetal calf serum, L-glutamine, penicillin−streptomycin, Liebovitz's K-15, MCDB135, and insulin, all purchased from Sigma-Aldrich.

Synthesis of PAAm-*g*-PFPA. The synthesis of the macromolecular adhesion promoter was performed by grafting perfluorophenyl azide *N*-hydroxysuccinimidyl ester onto a backbone of

poly(allyl amine) and has been described previously.[30] The adhesion promoter has a theoretical stoichiometry of one PFPA unit per four amines (see Figure 1A); however, a slightly lower grafting ratio is expected, according to previously published data.[30,33]

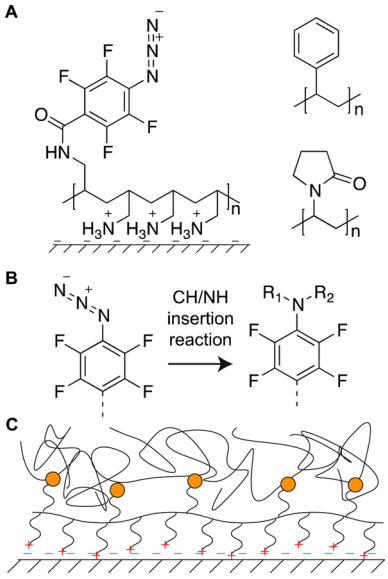

Figure 1. (A) PAAm-*g*-PFPA adhesion promoter electrostatically adsorbed onto a negatively charged substrate and chemical structures of polystyrene (upper) and poly(vinylpyrrolidone) (lower). (B) The decomposition of the azide upon UV exposure and/or heat forms a reactive nitrene capable of C−H/N−H insertion reactions, covalently linking a molecule to the adhesion promoter. (C) Schematic drawing of a randomly attached polymer to the adhesion-promoter molecule.

Homogenous Sample Preparation. Silicon substrates (POWATEC GmbH) and glass coverslips (thickness #3, approximately 0.3 μm, Gerhard Menzel GmbH) were ultrasonicated twice in toluene and twice in 2-propanol. Prior to surface functionalization, substrates were exposed to rf oxygen plasma (<0.04 mbar, power 100 W, 2 min, PDC-32G, Harrick Scientific) to impart a negative charge to the substrates and immersed in 0.1 mg/mL PAAm-*g*-PFPA 2:3 HEPES 1 (10 mM, pH:7.4):ethanol solution for 30 min. Wafers were rinsed twice in 2:3 HEPES 1:ethanol and then in ultrapure water (UPW, Milli-Q Advantage A10, Millipore) followed by blow-drying with filtered (ϕ = 0.22 μm) N_2 gas. Polymer solutions of PVP (25 mg/mL, chloroform) and PS (10 mg/mL, toluene) were prepared and spin-coated (2000 rpm, 40 s, 4000 rpm, 10 s) onto PAAm-*g*-PFPA-functionalized substrates. To covalently link the polymer chains to the azide (see Figure 1B), substrates were UV irradiated at 254 nm for 2 min (approximately 0.8 mW/cm^2, CAMAG). To remove nonattached polymer chains, PVP-covered substrates were rinsed in chloroform by overnight immersion, followed by exchange of the solvent, ultrasonication for 5 min, and finally exchange of solvent again and blow-drying. For PS the substrates were rinsed in ethyl acetate by ultrasonication for 10 min, followed by overnight immersion in fresh solvent, exchange of solvent, another round of ultrasonication for 10 min, and finally rinsing in ethyl acetate and blow-drying.

Micropattern Fabrication. To fabricate micropatterned samples, consisting of PS spots in a PVP background, samples were first prepared as described above for homogeneous PS; see Figure 2 for a description of the sample-preparation procedure. During UV exposure, the lamp was equipped with a honeycomb lighting grid (S 55°, Jinbei Photographic Equipment Co., Ltd.) to minimize angle spread in the UV output to less than 9° and to increase pattern uniformity. This reduced the light intensity to approximately 0.06 mW/cm^2. A chromium-on-quartz photolithography mask was placed on top of the substrates in contact mode and was held in place with magnets; see Table 1 for a list of pattern geometries used. Wafers were exposed for

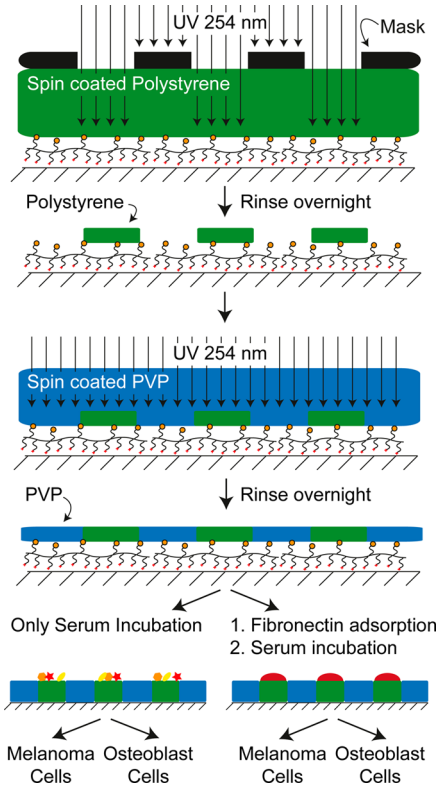

Figure 2. Schematic description of the fabrication route for adhesive micropatterns (polystyrene) in a nonadhesive background (PVP). Micropatterned substrates were tested either after incubation in complete medium containing fetal calf serum or after first immersing samples in a 10 μg/mL fibronectin solution followed by complete medium incubation prior to the cell-adhesion assay.

Table 1. Nominal Feature Sizes on the Mask, Protein-Adhesive Diameter of the Spots, and Effective PS Spot Diameter as Determined by TOF-SIMS

pattern index	nominal diameter (μm)	spacing (μm)	protein adhesive diameter (μm)[a]	ToF-SIMS "section IV" diameter (μm)[b]
P1	15	120	17.1 ± 0.8	16.5 ± 0.1
P2	20	150	20.8 ± 0.6	22.2 ± 0.2
P3	37.5	300	40.6 ± 0.9	38.8 ± 0.3
P4	75	600	77.6 ± 1.3	76.8 ± 0.2
P5	150	600	153.6 ± 1.7	151.2 ± 0.4

[a]Spot defined by BSA-TRITC adsorption (N = 34). [b]TOF-SIMS analysis of spots (N = 3); see Figure 4 for further information on how this region was defined.

5 min, a sufficiently long duration to ensure that a full monolayer of PS was formed within the spots (see Figure S2 of the Supporting Information for attachment kinetics). Unattached PS was rinsed off as described above for homogeneous PS. PVP was then applied, following the same protocol as for homogeneous PVP.

Adsorption of BSA-TRITC. Micropatterned glass coverslips were incubated for 1 h in 0.1 mg/mL BSA-TRITC dissolved in HEPES 2 buffer (10 mM, pH 7.4, 150 mM NaCl), rinsed twice in HEPES 2 buffer, rinsed in UPW, and blow-dried. Samples were characterized using an inverted epi-fluorescence microscope (Axiovert 200 M, Carl Zeiss AG), and grayscale images were collected.

Cell-Adhesion Assay. Immediately before the cell assay, samples were incubated in phosphate-buffered saline (PBS) for 20 min, followed by sterilization in a 7:3 ethanol/water mixture for 20 min, washed twice in sterile UPW and PBS, and incubated in PBS for 30

min at room temperature (rt). To enhance cell adhesion, half the samples were backfilled with fibronectin by immersion in 10 μg/mL fibronectin in PBS for 20 min at rt, washed twice in PBS, and incubated in complete medium (for SaOs-2, McCoy's 5A supplemented with 10% fetal calf serum, 1% L-glutamine, 1% penicillin–streptomycin; for WM 239, 1:4 Leibovitz's L-15:MCDB 135 supplemented with 2% fetal calf serum, 1% penicillin–streptomycin, 5 mg/mL insulin), at 37 °C for 20 min prior to cell-seeding. Samples that were not exposed to fibronectin solution were similarly incubated in complete medium containing serum before the cell assay. Melanoma (WM 239) or osteoblast (SaOs-2) cells were seeded at a concentration of 3×10^5 cells/sample. After 4 h, the samples were washed in PBS (37 °C) in order to remove nonadhered cells. The evolution of cell attachment was followed after 4 h (immediately after PBS wash), at 24 h, and at 48 h after incubation at 37 °C in a 5% CO_2 atmosphere. One replicate was fixed (4% formaldehyde, 4h) at each time point and characterized by phase-contrast microscopy (Axiovert 40, Carl Zeiss Microscopy GmbH).

Cytoskeleton Analysis. Cells were fixed with 4% formaldehyde after 24 h of culture and incubated in PBS–glycine (0.1 M) to permeabilize the cell membrane. Additionally, samples were immersed in a blocking buffer to block nonspecific sites. AlexaFluor 488 phalloidin (Molecular probes, Life Technologies) was used to label F-actin,[50] while DAPI (4′,6-diamidino-2-phenylindole, Molecular Probes, Life Technologies) was used to label the DNA in the cell nuclei. To visualize the distribution of focal adhesions, immunostaining against vinculin was performed with a primary antibody against vinculin (anti-h vinculin monoclonal antibody produced in mouse, Sigma-Aldrich) and observed with a fluorescently tagged secondary antibody [antimouse F(ab)2 fragment-Cy3, Sigma-Aldrich]. After staining, samples were stored in a mounting medium (Mowiol, Sigma-Aldrich) for preservation and to avoid photobleaching. Samples were analyzed by confocal microscopy (Leica Microsystems).

X-ray Photoelectron Spectroscopy. To confirm the formation of the PAAm-*g*-PFPA self-assembled monolayer and the subsequent immobilization of PVP and PS, X-ray photoelectron spectroscopy (XPS) was performed. Data were collected on a VG Theta Probe spectrometer (Thermo Scientific). The emission angle was 53° with an acceptance angle of ±30°. A monochromatic 200 W Al K α source with a spot size of 400 μm was used. Survey spectra and high-resolution spectra (C 1s, N 1s, O 1s, F 1s, Si 2p) were collected at pass energies of 200 and 100 eV, respectively. Samples were measured after plasma treatment, formation of the PAAm-*g*-PFPA self-assembled monolayer, and after polymer immobilization. On the PAAm-*g*-PFPA coating, N 1s spectra were collected first and last, to determine any sample degradation of the azide during X-ray exposure.

Time-of-Flight Secondary Ion Mass Spectrometry. For laterally resolved chemical characterization of the micropatterns, time-of-flight secondary ion mass spectrometry (ToF-SIMS V, ION-TOF GmbH) was used in burst-alignment mode with a lateral resolution of approximately 500 nm. Spectra were collected using a Bi_3^{2+} cluster beam with a target current of 0.07 pA at 60 μs cycle time (mass range 0–312 m/z). Total dose density was estimated to be 8×10^{11} ions/cm^2—well below the established limit of 1×10^{13} ions/cm^2 for static SIMS.[51] Spectra processing and peak selection were carried out with Surfacelabs (v. 6.3.56454, ION-TOF GmbH), and spectral analysis and image reconstruction were performed in Matlab (R2013b, MathWorks) using custom algorithms. All spectra were mass calibrated using the C^+, CH^+, CH_2^+, $C_2H_3^+$, and $C_3H_5^+$ peaks.

RESULTS AND DISCUSSION

Chemical Composition of Homogeneous Films. The formation of the self-assembled monolayer of PAAm-*g*-PFPA and the subsequent photochemical immobilization of PVP and PS were confirmed by XPS on homogeneous samples (see Figure 3A). The results are in good agreement with previously published data.[33] In brief, functionalization of silicon wafers with PAAm-*g*-PFPA was confirmed by the presence of fluorine and nitrogen (a detailed analysis of the N 1s envelope is given below). Upon immobilization of PVP, the fluorine signal disappears, and the silicon signal is barely detectable, while nitrogen, oxygen, and carbon are present, representative of PVP. The PS coating displays a single carbon peak, as expected. The presence of a silicon signal on the PVP coating is likely to be due to differences in the polymer film thickness between PS and PVP—approximately 6–7 vs 5–6 nm, as previously determined.[33] The silicon signal is less attenuated in the case of the PVP film; however, fluorine is not detected, which is explained by the fluorine concentration lying below the detection limit of the instrument. This provides an indication that the polymer monolayers were largely defect free and that the PAAm-*g*-PFPA is localized on the substrate throughout the surface preparation.

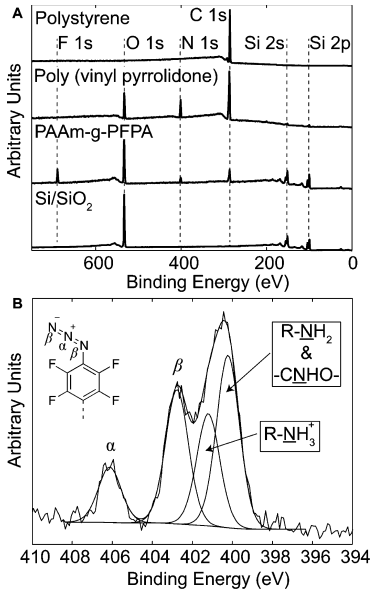

Figure 3. (A) Survey spectra of SiO_2, PAAm-*g*-PFPA, PVP, and PS (from bottom to top). The adsorption of PAAm-*g*-PFPA is evident from the presence of fluorine and nitrogen. After immobilization of PVP, the presence of nitrogen, oxygen, and carbon is detected, as expected. In the PS coating, only carbon is detected. The fluorine peak disappears after immobilization of PS and PVP, while a minute silicon signal can be detected on the PVP, but not on the PS, coating. This indicates a confluent polymer film on top of the PAAm-*g*-PFPA adhesion promoter. (B) High-resolution N 1s spectrum after adsorption of PAAm-*g*-PFPA. Two nitrogen signals, denoted α and β, are associated with the azide,[53] and the two peaks at lower binding energies are associated with primary amine or amide and protonated primary ammonium groups.[54]

Figure 3B shows the high-resolution N 1s spectrum of a self-assembled monolayer of PAAm-*g*-PFPA on a silicon substrate. Four peaks, with fwhm of 1.35 ± 0.01 eV, were fitted to the envelope at binding energies 400.18 ± 0.06, 401.11 ± 0.08, 402.73 ± 0.03, and 406.17 ± 0.03 eV. The peak at 400.18 eV was assigned to primary amine and amide (from grafting of PFPA) and the peak at 401.11 eV to protonated ammonium groups,[52] both belonging to poly(allyl amine). The two peaks at higher binding energy are in agreement with previously published spectra of PFPA,[53] thus confirming the presence of the azide. The central azide nitrogen, being electron-deficient, was assigned to 406.17 eV, denoted α in Figure 3B. The two outer nitrogen atoms share a delocalized negative charge, and the signal was positioned at 402.73 eV, denoted β. The area ratio between the α and β nitrogen was 1:2.6, slightly larger

than the expected 1:2 ratio. However, analysis of UV-irradiated PAAm-*g*-PFPA still reveals a peak at 402 eV, while no peak can be seen at 406 eV (see Supporting Information, Figures S2 and S3), indicating that the azide was decomposed and no longer detectable and that the remaining signal at 402 eV could be due to small amounts of oxidized nitrogen.[54]

Micropattern Characterization. TOF-SIMS image spectra were collected on micropatterned glass coverslips to analyze the lateral distribution of PS and PVP. A 50 × 50 μm^2 image of a spot of nominal diameter 20 μm, pattern P2, serves as an example for the following discussion. Two peak sets of molecular fragments representative of PS and PVP have previously been established[33] and were applied to the interpretation of the image spectra. To classify pixels in the image associated with PS, PVP, or a mixture of the two, an approach suggested by Gilmore et al. and Lee et al. was employed.[55,56] In every pixel, the total number of counts in each peak list was summed, normalized to the maximum number of counts within the peak list (to account for differences in the secondary-ion yield between the two polymers), and plotted against one another (see Figure 4A). Two main pixel clusters can be discerned, connected by a domain of intermediate peak-intensity ratios. To generate an unambiguous criterion for sorting pixels into either PS or PVP, a bisector line is drawn through the midpoint between centers of the two clusters.[55] To simplify the categorization of pixels, a plot displaying the frequency of pixels as a function of angle was established and shown in Figure 4B.[56] Two roughly Gaussian distributions can be recognized, with means at 10° and 84° and fwhm of 6 and 5, respectively, determined by manual spectrum analysis. The peak means are not at 0° and 90°, since the molecular fragments selected for analysis do have some overlap between the two polymers. Assuming a normal distribution, the standard deviation of the means (SD) were ±2.55° and ±2.12°, respectively. The boundaries of each peak were defined by taking the mean ±3SD, thus providing upper and lower limits for section I (17.65°), representative of PVP, and section IV (77.64°), representative of PS. The remaining pixels were categorized as either mixed with a high concentration of PVP (section II) or mixed with a high concentration of PS (section III), separated by the bisector position (45.8°). The classified spectrum was then reconstructed into the image displayed in Figure 4C. The spot consisting of PS is clearly visible, in addition to a corona, representing pixels coming from sections II and III, located around the spot, indicating a short gradient in composition at the spot periphery. The width of the corona was approximately 4 pixels, or 1.6 μm. The effective lateral resolution of the instrument was approximately 500−600 nm, determined on coplanar patterns of gold and titanium,[57] indicating that the corona represented a true chemical gradient and was not a consequence of blurring of a distinct interface. This was also confirmed by atomic force microscopy (see the Supporting Information, Figure S6).

To ensure that the pixels classified as sections I and IV consisted of pure PVP and PS, respectively, the ratio of the non-normalized PS-to-PVP peak intensities was also calculated and compared with the same ratio from reference spectra on homogeneous PS and PVP:

$$PS_{Frac} = \frac{I_{PS}}{I_{PS} + I_{PVP}}$$

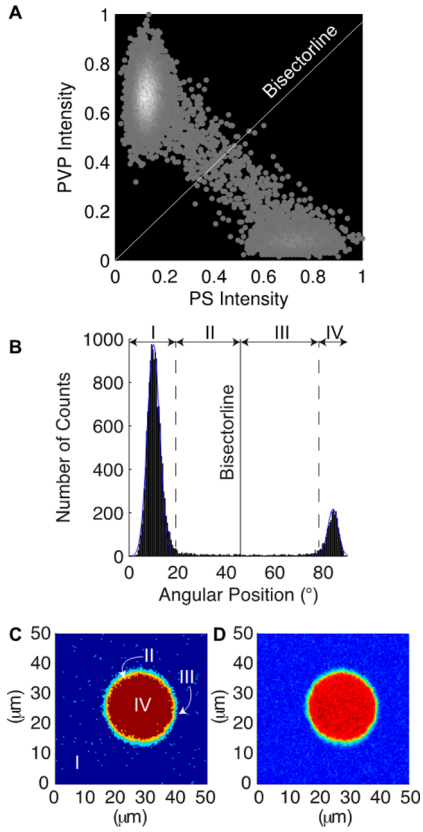

Figure 4. TOF-SIMS characterization of a representative 20 μm micropattern spot. (A) Graph displaying the distribution of pixels representing normalized PVP-to-PS intensity ratios for all pixels. The grayscale intensity represents the frequency of occurrence, with a brighter color representing a larger number of pixels.[55] (B) The number of counts per pixel plotted against the angular position in graph A.[56] Overlaid are two Gaussian curves indicating the limits assigned to PVP (section I) and PS (section IV) regions. Sections II and III are representative of pixels of mixed composition and divided by the bisector position. (C) Reconstructed TOF-SIMS image with the classification of pixels from the sections in panel B. (D) The fraction of PS as calculated from the ratio of PS to PVP representative peaks.

where I_{PS} is the sum of PS representative peak intensities and I_{PVP} is the sum of PVP representative peak intensities. The reconstructed image, displaying PS_{Frac}, is shown in Figure 4D. The average PS_{Frac} in sections I and IV was 0.15 and 0.90, respectively, to be compared with the corresponding value of 0.18 and 0.97 obtained for the reference spectra of PS and PVP, indicating a close-to-pure composition within the spot and outside of the corona. The larger discrepancy between the PS fractions within the spot and the PS reference can be explained by lower signal-to-noise ratio due the lower number of pixels representing PS composition in a 20 μm spot within a 50 × 50 μm^2 field of view. The corresponding ratios for sections I and IV on the 35 μm nominal spot diameter (pattern P3) image (same field of view) were 0.18 and 0.95, respectively.

To determine the diameter of the spot, the number of pixels contained within each section was counted, and the area of the spot was calculated from the pixel size (0.15 μm^2). The diameter of the area enclosed by section I pixels (see Figure 4C) was 21.4 μm (see Table 1 for the other spot sizes). The PS region was thus enlarged compared to the mask pattern, excluding the width of the corona of 1.6 μm.

dx.doi.org/10.1021/am5042093 | ACS Appl. Mater. Interfaces 2014, 6, 18683−18692

Adsorption of BSA-TRITC on Micropatterns. Micropatterned coverslips were incubated in BSA-TRITC to visualize the pattern geometry under fluorescence microscopy and to quantify the diameter of the protein-adhesive spot. BSA was found to adsorb preferentially on the PS spots, illustrating that the PVP coating was able to resist nonspecific protein adsorption. The nonfouling action of PVP has previously been reported, both in situ using quartz-crystal microbalance and ex situ with ellipsometry[30] and by quantifying the adsorbed amount of ^{125}I-tagged proteins[48] by means of radioactive decay. Spot diameters were characterized in ImageJ (64-bit, http://rsbweb.nih.gov/ij/)[58] by measuring the extent of the protein-adhesive region in six spots over four fields of view. Spots of 20 and 37.5 μm nominal diameter had effective diameters of 20.8 $\pm$ 0.6 and 40.6 $\pm$ 0.9 μm, respectively (see Figure 5 and Table 1), indicating an enlargement of the effective pattern diameter by approximately 1−3 μm during fabrication.

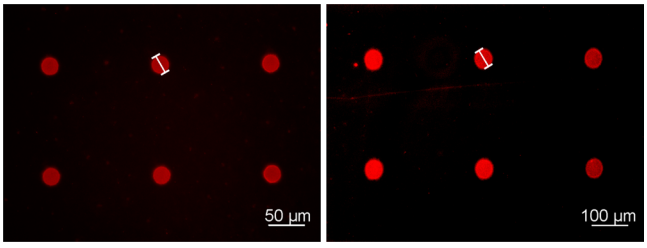

Figure 5. False-color images showing BSA-TRITC adsorption on PS/PVP micropatterned glass coverslips. Spots have 20 μm (left) and 37.5 μm (right) nominal diameter. Spot diameters were determined by manually measuring the size of the protein-adhesive regions.

Pattern Reproduction during Fabrication. During micropatterning, data from TOF-SIMS and protein adsorption indicated that the effective pattern diameter was larger on the surface compared to the mask. Further, the pattern broadening was confirmed by atomic force microscopy at the edge of a pattern (see the Supporting Information, Figure S6). The diameter of the spot, as defined by "section IV" pixels (see Figure 4), corresponded most closely with the size of the protein-adhesive region, while inclusion of pixels from sections II and III led to larger deviations. This is probably due to low adsorption of proteins within the corona region, which thus has little influence on the determination of the protein-adhesive diameter.

The pattern broadening could be a consequence of using a noncollimated light source, despite the presence of a lighting grid. However, the undercut region that would result due to scattering, considering photons impinging at a maximum angle of 9° to the surface normal, would only be approximately 13 nm (spin-coated film was approximately 85 nm). More probable are multiple reflections between the chromium mask and the glass substrate, combined with the sensitivity of the photochemical system where, theoretically, a single photon can provoke the immobilization of an entire polymer chain. This hypothesis is also strengthened by the fact that the absolute size of the corona appears independent of the nominal pattern diameter (see the Supporting Information, Table S4). The broadening effect could possibly be mitigated by shortening the UV exposure time, however, with the drawback of risking a mixed chemical composition inside the spot due to underexposure (see the Supporting Information, Figures S3 and S5).

Adhesion of Melanoma and Osteoblast Cells. Phase-contrast images of melanoma (WM 239) and osteoblast (SaSo-2) cells on nominal ϕ = 20 μm micropatterns are shown in Figure 6. After 4 h, nonadhered cells were washed off, and cell behavior was observed at 24 and 48 h. Patterns were tested after being backfilled with fibronectin, followed by serum incubation, or after only serum incubation (see Figure 2). Spots incubated with fibronectin had an increased attachment yield (the fraction of spots occupied by one or more cells) and retained a higher number of cells during cell proliferation (see Figure 7). It should be noted that on samples without fibronectin, on which the protein mixture of the serum is expected to adsorb to the PS spots, both cell types adhered weakly. This difference could be attributed to a lower density of cell-adhesive proteins on the spots adsorbed from serum, compared to those exposed to 10 μg/mL FN prior to serum incubation. In particular, it has been reported that neither fibronectin nor vitronectin adsorb in sufficiently high density from complete cell-culture medium (including serum) on hydrophobic PS to promote cell adhesion.[59−61] Due to the

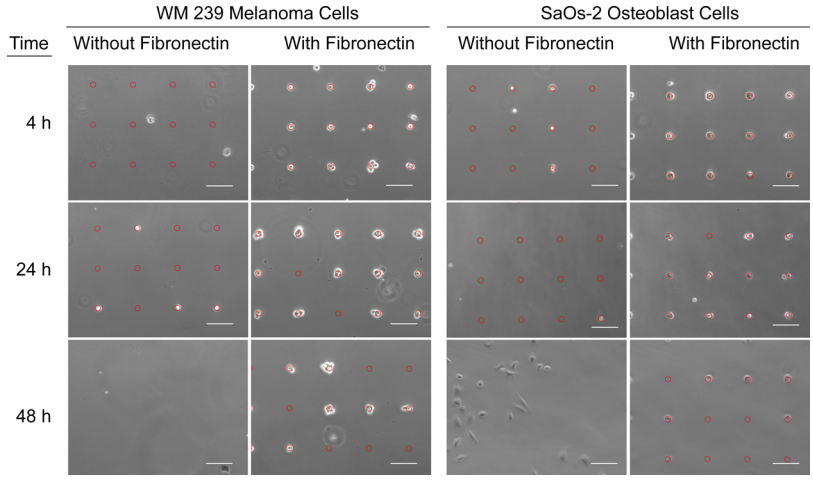

Figure 6. Phase-contrast images showing cell adhesion on 20 μm spots at different times after cell seeding. Melanoma cells and osteoblasts adhered explicitly on adhesive regions, while being unable to attach on the PVP background. Fibronectin backfilling increased the attachment yield and, notably, prevented detachment during cell proliferation. Overlays in red circles represent the mask-pattern positions aligned to the cell lattice. Scale bar: 100 μm.

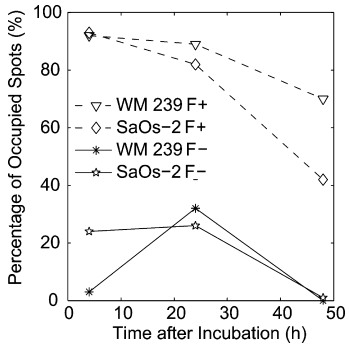

Figure 7. Percentage of spots averaged over 6 fields of view, containing 48 spots each, occupied by one or more cells with or without fibronectin at different time points. Fibronectin (+F) increases both the initial number of spots occupied by cells as well as the cells retained on the adhesive spot. In comparison, only ~30% of the spots are occupied by cells without fibronectin (−F). After 48 h, cells start to desorb from the spots, possibly during mitosis.

lower adhesion strength on samples not preincubated in fibronectin, the number of occupied spots became a strong function of protocol and sample handling. This is particularly true in the case of WM 239 cells and provides an explanation as to the seemingly unintuitive increase in the fraction of occupied spots from 4 to 24 h (see Figure 7). The lower number of cells confined to the lattice after 4 h is therefore attributed to sample-handling variability. It should be noted that in Figure 7 the fraction of spots occupied by a cell is presented; cells not confined to the lattice were ignored. Patterns not backfilled with fibronectin retained no cells after 48 h. Precoating samples with fibronectin was found to be more efficient in retaining cells, compared to relying on protein adsorption from the serum.

The actin fibers formed a ring around the nucleus on surfaces both with and without fibronectin (see Figure 8). Moreover the actin proteins appeared to be organized in thick and well-defined fibers. For small spot diameters, cells occupied the entire available surface, adopting the shape of the PS microdomain. In contrast, on larger spot diameters, where the border of the spot did not constitute a direct confinement,

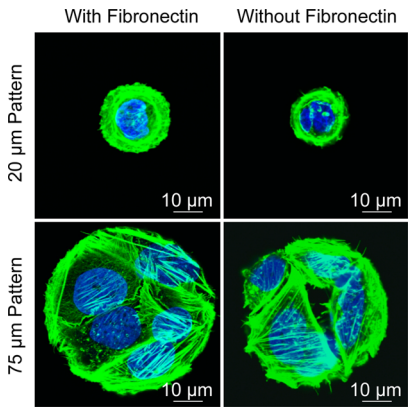

Figure 8. Confocal images of F-actin distribution (green) and nuclei (blue). Actin fibers form a ring around the nucleus on both surfaces with and without fibronectin (top). When cells attach to adhesive regions larger than the cell size, they spread and assume different morphologies. The actin cytoskeleton forms thick and well-defined actin fibers (bottom).

cells spread and assumed several different morphologies, as observable from the cytoskeleton analysis (Figure 8). Immunostaining against vinculin, a marker for focal adhesions,[62,63] revealed that the adhesive points were more elongated and that the fluorescence intensity, which is linearly related to the applied forces, was higher on samples backfilled with fibronectin, confirming that the adhesive forces were stronger on fibronectin-coated samples (see Figure 9).

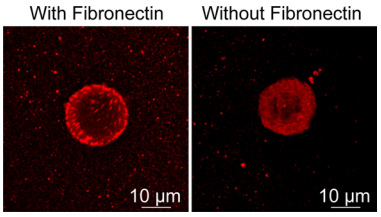

Figure 9. Confocal images of focal adhesions of SaOs-2 cells. Focal adhesions are elongated, and the fluorescence intensity is higher when cells grow on substrates with fibronectin (left).

The difference between spots that were preincubated with fibronectin or not is still evident at 48 h, indicating that fibronectin has not been displaced. Fibronectin has previously been shown to adsorb irreversibly onto hydrophobic surfaces.[64] However, cells are capable of both remodeling the fibronectin film in the cell-contact area as well as internalizing the protein through endocytosis.[65] Indeed, Fink et al. observed that it was necessary to covalently link fibronectin to the substrate in order to prevent cells (retinal pigment epithelium cells) from peeling off the protein film.[37] However, this could have been a consequence of using patterns where cells spread across nonadhesive regions and thus imparted greater stress to the underlying material. It is unclear whether the same scenario would occur in our system if more complex pattern geometries had been tested, as the stability of the physisorbed protein film also depends on the physical-chemical properties of the underlying interface.[64,66] Furthermore, the cell−fibronectin interaction has been reported to be complex, as the cellular response depends both on the fibronectin conformation in the adsorbed film,[67−69] which is altered by the surface characteristics,[70,71] and whether fibronectin is covalently immobilized or physisorbed.[72] In the present study, we are mostly concerned with initial cell adhesion, and thus, the reproducible ability of the fibronectin-backfilled micropatterns to provide a cell-adhesive environment indicates that the physisorbed protein layer remains sufficiently stable and biologically active for the duration of the assay.

Coating Stability. Cells cultivated on micropatterned samples with fibronectin were unable to spread onto the inert background, even after 48 h. However, on samples without fibronectin, SaOs-2 cells that had desorbed from the polystyrene spots during mitosis appeared capable of reattaching onto the PVP background. In contrast, WM 239 cells do not appear to be able to spread on PVP under similar conditions. This might indicate an intrinsic propensity of osteoblasts to form a stronger cell−substrate interaction—a hypothesis strengthened by the observation by Ernst et al. that osteosarcoma cells adhered more strongly than fibroblasts on a thermoresponsive polymer coating.[73] It thus appears that the long-term capability of the inert background to prevent cell spreading is cell-type dependent and intimately linked with the intensity of the adhesive interaction within the micropattern.

The pattern longevity will be important when considering possible applications. In the present study, the assay time was limited to a maximum of 48 h. After this time point, the majority of the cells will have undergone cell division, and thus, the concept of single cells does not apply. However, within this time frame a variety of experimental studies could be conducted to explore areas such as cell adhesion, cell elasticity, and cell morphogenesis, as well as the influence of drugs and toxins on these cellular processes.

During UV activation of the azide, two scenarios can occur: insertion into a macromolecule within close proximity or cross-linking between PAAm-*g*-PFPA molecules. The latter will lead to a cross-linked macromolecular network, which is not easily displaced due to the increased number of surface interactions per polymer, all of which would have to be simultaneously broken for displacement to occur.[74] This is an advantage over other physisorbed macromolecular systems, such as PLL-*g*-PEG, which only has a limited number of substrate interactions. A further advantage of PVP versus PEG-based systems is its inherently higher resistance toward oxidative breakdown.[24] From the results in the present study we show that PVP is a potentially very useful replacement for PEG where a nonfouling interface is desired, especially in challenging environments, such as cell media, or for long-term applications.

CONCLUSION

Photochemically prepared polymer micropatterns of polystyrene, employing poly(vinylpyrrolidone) as the inert background, have been shown to form a stable and reproducible platform for confining cells on a 2D lattice. Backfilling of the polystyrene microdomains with fibronectin provided improved cell adhesion, possibly through RGD-integrin mediated interactions, but it was not strictly necessary for cell confinement. The presented platform is versatile with regard to cell type, with both melanoma and osteoblasts adhering on the micropatterns, and combined with the inert background, the platform allows backfilling of other cell-adhesive proteins, such as laminin or collagen, to target other cell types or to mimic different tissue environments. Photochemically immobilized PVP has proven efficient in preventing cell adhesion and constitutes an excellent alternative to PEG in biological applications. Furthermore, the photochemical immobilization route is adaptable with regard to polymer choice, and consequently, the chemistry within and outside the pattern can readily be varied.

ASSOCIATED CONTENT

Supporting Information

N 1s XPS data on PAAm-*g*-PFPA after X-ray and UV exposure, kinetics of the PS immobilization, protein-adhesive diameter and fluorescence-intensity variation with different UV exposure times, summary of the TOF-SIMS characterization of the micropattern geometry, and topography map over the edge of a pattern. This material is available free of charge via the Internet at http://pubs.acs.org.

AUTHOR INFORMATION

Corresponding Author

*E-mail: nspencer@ethz.ch.

Notes

The authors declare the following competing financial interest(s): Drs. Zürcher and Tosatti are founders of SuSoS AG, which manufactures one of the chemicals used in the process described. This material is commercially available, however, and openly described by them and others in the literature. Prof. Spencer is president of the scientific advisory board of SuSoS AG.

ACKNOWLEDGMENTS

This work was supported by the European Commission 7th Framework Program SEACOAT FP7/2007-2013 and by the CTI Innovation Cheques Program (CTI no. 14919 INNO-12-LS:SPACES).

REFERENCES

(1) Thery, M. Micropatterning as a Tool To Decipher Cell Morphogenesis and Functions. *J. Cell Sci.* **2010**, *123*, 4201−4213.
(2) Théry, M.; Pépin, A.; Dressaire, E.; Chen, Y.; Bornens, M. Cell Distribution of Stress Fibres in Response to the Geometry of the Adhesive Environment. *Cell Motil. Cytoskeleton* **2006**, *63*, 341−355.
(3) Anderegg, F.; Geblinger, D.; Horvath, P.; Charnley, M.; Textor, M.; Addadi, L.; Geiger, B. Substrate Adhesion Regulates Sealing Zone Architecture and Dynamics in Cultured Osteoclasts. *PLoS One* **2011**, *6*, e28583.
(4) Singhvi, R.; Kumar, A.; Lopez, G. P.; Stephanopoulos, G. N.; Wang, D.; Whitesides, G. M.; Ingber, D. E. Engineering Cell-Shape and Function. *Science* **1994**, *264*, 696−698.
(5) Reymann, A.-C.; Martiel, J.-L.; Cambier, T.; Blanchoin, L.; Boujemaa-Paterski, R.; Théry, M. Nucleation Geometry Governs Ordered Actin Networks Structures. *Nat. Mater.* **2010**, *9*, 827−832.
(6) Théry, M.; Racine, V.; Piel, M.; Pépin, A.; Dimitrov, A.; Chen, Y.; Sibarita, J.-B.; Bornens, M. Anisotropy of Cell Adhesive Microenvironment Governs Cell Internal Organization and Orientation of Polarity. *Proc. Natl. Acad. Sci. U. S. A.* **2006**, *103*, 19771−19776.
(7) Kilian, K. A.; Bugarija, B.; Lahn, B. T.; Mrksich, M. Geometric Cues for Directing the Differentiation of Mesenchymal Stem Cells. *Proc. Natl. Acad. Sci. U. S. A.* **2010**, *107*, 4872−4877.
(8) McBeath, R.; Pirone, D. M.; Nelson, C. M.; Bhadriraju, K.; Chen, C. S. Cell Shape, Cytoskeletal Tension, and RhoA Regulate Stem Cell Lineage Commitment. *Dev. Cell* **2004**, *6*, 483−495.
(9) Théry, M.; Racine, V.; Pépin, A.; Piel, M.; Chen, Y.; Sibarita, J.-B.; Bornens, M. The Extracellular Matrix Guides the Orientation of the Cell Division Axis. *Nat. Cell Biol.* **2005**, *7*, 947−953.
(10) Jiang, X. Y.; Bruzewicz, D. A.; Wong, A. P.; Piel, M.; Whitesides, G. M. Directing Cell Migration with Asymmetric Micropatterns. *Proc. Natl. Acad. Sci. U. S. A.* **2005**, *102*, 975−978.
(11) Brock, A.; Chang, E.; Ho, C.-C.; LeDuc, P.; Jiang, X.; Whitesides, G. M.; Ingber, D. E. Geometric Determinants of Directional Cell Motility Revealed Using Microcontact Printing. *Langmuir* **2003**, *19*, 1611−1617.
(12) Falconnet, D.; Csucs, G.; Grandin, H. M.; Textor, M. Surface Engineering Approaches to Micropattern Surfaces for Cell-Based Assays. *Biomaterials* **2006**, *27*, 3044−3063.
(13) Ekblad, T.; Liedberg, B. Protein Adsorption and Surface Patterning. *Curr. Opin. Colloid Interface Sci.* **2010**, *15*, 499−509.
(14) Zhao, B.; Brittain, W. Polymer Brushes: Surface-Immobilized Macromolecules. *Prog. Polym. Sci.* **2000**, *25*, 677−710.
(15) Elbert, D. L.; Hubbell, J. A. Self-Assembly and Steric Stabilization at Heterogeneous, Biological Surfaces Using Adsorbing Block Copolymers. *Chem. Biol. (Oxford, U. K.)* **1998**, *5*, 177−183.
(16) Kenausis, G. L.; Vörös, J.; Elbert, D. L.; Huang, N.; Hofer, R.; Ruiz-Taylor, L.; Textor, M.; Hubbell, J. A.; Spencer, N. D. Poly(L-lysine)-*g*-poly(ethylene glycol) Layers on Metal Oxide Surfaces: Attachment Mechanism and Effects of Polymer Architecture on Resistance to Protein Adsorption. *J. Phys. Chem. B* **2000**, *104*, 3298−3309.
(17) Pasche, S.; De Paul, S.; Voros, J.; Spencer, N.; Textor, M. Poly(L-lysine)-*graft*-poly(ethylene glycol) Assembled Monolayers on Niobium Oxide Surfaces: A Quantitative Study of the Influence of Polymer Interfacial Architecture on Resistance to Protein Adsorption by ToF-SIMS and in Situ OWLS. *Langmuir* **2003**, *19*, 9216−9225.

(18) Azioune, A.; Storch, M.; Bornens, M.; Théry, M.; Piel, M. Simple and Rapid Process for Single Cell Micro-Patterning. *Lab Chip* **2009**, *9*, 1640.
(19) Michel, R.; Lussi, J. W.; Csucs, G.; Reviakine, I.; Danuser, G.; Ketterer, B.; Hubbell, J. A.; Textor, M.; Spencer, N. D. Selective Molecular Assembly Patterning: A New Approach to Micro- and Nanochemical Patterning of Surfaces for Biological Applications. *Langmuir* **2002**, *18*, 3281−3287.
(20) Falconnet, D.; Koenig, A.; Assi, F.; Textor, M. A Combined Photolithographic and Molecular-Assembly Approach To Produce Functional Micropatterns for Applications in the Biosciences. *Adv. Funct. Mater.* **2004**, *14*, 749−756.
(21) Lussi, J.; Falconnet, D.; Hubbell, J.; Textor, M.; Csucs, G. Pattern Stability Under Cell Culture Conditions—A Comparative Study of Patterning Methods Based on PLL-*g*-PEG Background Passivation. *Biomaterials* **2006**, *27*, 2534−2541.
(22) Chen, Y.; Pidhatika, B.; von Erlach, T.; Konradi, R.; Textor, M.; Hall, H.; Lühmann, T. Comparative Assessment of the Stability of Nonfouling Poly(2-methyl-2-oxazoline) and Poly(ethylene glycol) Surface Films: An in Vitro Cell Culture Study. *Biointerphases* **2014**, *9*, 031003.
(23) Blättler, T. M.; Pasche, S.; Textor, M.; Griesser, H. J. High Salt Stability and Protein Resistance of Poly(L-lysine)-*g*-poly(ethylene glycol) Copolymers Covalently Immobilized via Aldehyde Plasma Polymer Interlayers on Inorganic and Polymeric Substrates. *Langmuir* **2006**, *22*, 5760−5769.
(24) Konradi, R.; Acikgoz, C.; Textor, M. Polyoxazolines for Nonfouling Surface Coatings—A Direct Comparison to the Gold Standard PEG. *Macromol. Rapid Commun.* **2012**, *33*, 1663−1676.
(25) Sharma, S.; Johnson, R. W.; Desai, T. A. Evaluation of the Stability of Nonfouling Ultrathin Poly(ethylene glycol) Films for Silicon-Based Microdevices. *Langmuir* **2004**, *20*, 348−356.
(26) Ogaki, R.; Zoffmann Andersen, O.; Jensen, G. V.; Kolind, K.; Kraft, D. C. E.; Pedersen, J. S.; Foss, M. Temperature-Induced Ultradense PEG Polyelectrolyte Surface Grafting Provides Effective Long-Term Bioresistance against Mammalian Cells, Serum, and Whole Blood. *Biomacromolecules* **2012**, *13*, 3668−3677.
(27) Prucker, O.; Naumann, C. A.; Rühe, J.; Knoll, W.; Frank, C. W. Photochemical Attachment of Polymer Films to Solid Surfaces via Monolayers of Benzophenone Derivatives. *J. Am. Chem. Soc.* **1999**, *121*, 8766−8770.
(28) Navarro, R.; Pérez Perrino, M.; Prucker, O.; Rühe, J. Preparation of Surface-Attached Polymer Layers by Thermal or Photochemical Activation of A-Diazoester Moieties. *Langmuir* **2013**, *29*, 10932−10939.
(29) Liu, L.-H.; Yan, M. Perfluorophenyl Azides: New Applications in Surface Functionalization and Nanomaterial Synthesis. *Acc. Chem. Res.* **2010**, *43*, 1434−1443.
(30) Serrano, Â.; Sterner, O.; Mieszkin, S.; Zuercher, S.; Tosatti, S.; Callow, M. E.; Callow, J. A.; Spencer, N. D. Nonfouling Response of Hydrophilic Uncharged Polymers. *Adv. Funct. Mater.* **2013**, *23*, 5706−5718.
(31) Wang, H.; Li, L.; Tong, Q.; Yan, M. Evaluation of Photochemically Immobilized Poly(2-ethyl-2-oxazoline) Thin Films as Protein-Resistant Surfaces. *ACS Appl. Mater. Interfaces* **2011**, *3*, 3463−3471.
(32) Wang, H.; Ren, J.; Hlaing, A.; Yan, M. Fabrication and Anti-Fouling Properties of Photochemically and Thermally Immobilized Poly(ethylene oxide) and Low Molecular Weight Poly(ethylene glycol) Thin Films. *J. Colloid Interface Sci.* **2011**, *354*, 160−167.
(33) Sterner, O.; Serrano, Â.; Mieszkin, S.; Zuercher, S.; Tosatti, S.; Callow, M. E.; Callow, J. A.; Spencer, N. D. Photochemically Prepared, Two-Component Polymer-Concentration Gradients. *Langmuir* **2013**, *29*, 13031−13041.
(34) Bielecki, R. M.; Doll, P.; Spencer, N. D. Ultrathin, Oil-Compatible, Lubricious Polymer Coatings: A Comparison of Grafting-to and Grafting-from Strategies. *Tribol. Lett.* **2012**, *49*, 273−280.
(35) Bartlett, M.; Yan, M. Fabrication of Polymer Thin Films and Arrays with Spatial and Topographical Controls. *Adv. Mater.* **2001**, *13*, 1449−1451.
(36) Yan, M.; Bartlett, M. Micro/Nanowell Arrays Fabricated From Covalently Immobilized Polymer Thin Films on a Flat Substrate. *Nano Lett.* **2002**, *2*, 275−278.
(37) Fink, J.; Th ry, M.; Azioune, A.; Dupont, R.; Chatelain, F. O.; Bornens, M.; Piel, M. Comparative Study and Improvement of Current Cell Micro-Patterning Techniques. *Lab Chip* **2007**, *7*, 672.
(38) Petersen, S.; Loschonsky, S.; Prucker, O.; Rühe, J.; Biesalski, M. Cell Micro-Arrays From Surface-Attached Peptide−Polymer Monolayers. *Phys. Status Solidi A* **2009**, *206*, 468−473.
(39) Liu, X.; Xu, Y.; Wu, Z.; Chen, H. Poly(*N*-vinylpyrrolidone)-Modified Surfaces for Biomedical Applications. *Macromol. Biosci.* **2013**, *13*, 147−154.
(40) Smith, L. E.; Rimmer, S.; MacNeil, S. Examination of the Effects of Poly(*N*-vinylpyrrolidinone) Hydrogels in Direct and Indirect Contact with Cells. *Biomaterials* **2006**, *27*, 2806−2812.
(41) Yanez, F.; Concheiro, A.; Alvarez-Lorenzo, C. Macromolecule Release and Smoothness of Semi-Interpenetrating PVP-PHEMA Networks for Comfortable Soft Contact Lenses. *Eur. J. Pharm. Biopharm.* **2008**, *69*, 1094−1103.
(42) Reimer, K.; Vogt, P. M.; Broegmann, B.; Hauser, J.; Rossbach, O.; Kramer, A.; Rudolph, P.; Bosse, B.; Schreier, H.; Fleischer, W. An Innovative Topical Drug Formulation for Wound Healing and Infection Treatment: In Vitro and in Vivo Investigations of a Povidone-Iodine Liposome Hydrogel. *Dermatology (Basel, Switz.)* **2000**, *201*, 235−241.
(43) Lee, J. Intrinsic Adhesion Properties of Poly(vinyl pyrrolidone) to Pharmaceutical Materials: Humidity Effect. *Macromol. Biosci.* **2005**, *5*, 1085−1093.
(44) Francois, P.; Vaudaux, P.; Nurdin, N.; Mathieu, H. J.; Descouts, P.; Lew, D. P. Physical and Biological Effects of a Surface Coating Procedure on Polyurethane Catheters. *Biomaterials* **1996**, *17*, 667−678.
(45) Wetzels, G.; Koole, L. H. Photoimmobilisation of Poly(*N*-vinylpyrrolidinone) as a Means To Improve Haemocompatibility of Polyurethane Biomaterials. *Biomaterials* **1999**, *20*, 1879−1887.
(46) Liu, X.; Sun, K.; Wu, Z.; Lu, J.; Song, B.; Tong, W.; Shi, X.; Chen, H. Facile Synthesis of Thermally Stable Poly(*N*-vinylpyrrolidone)-Modified Gold Surfaces by Surface-Initiated Atom Transfer Radical Polymerization. *Langmuir* **2012**, *28*, 9451−9459.
(47) Lu, X.; Gong, S.; Meng, L.; Li, C.; Yang, S.; Zhang, L. Controllable Synthesis of Poly(*N*-vinylpyrrolidone) and Its Block Copolymers by Atom Transfer Radical Polymerization. *Polymer* **2007**, *48*, 2835−2842.
(48) Wu, Z.; Chen, H.; Liu, X.; Zhang, Y.; Li, D.; Huang, H. Protein Adsorption on Poly(*N*-vinylpyrrolidone)-Modified Silicon Surfaces Prepared by Surface-Initiated Atom Transfer Radical Polymerization. *Langmuir* **2009**, *25*, 2900−2906.
(49) Liu, X.; Wu, Z.; Zhou, F.; Li, D.; Chen, H. Poly(vinylpyrrolidone-*b*-styrene) Block Copolymers Tethered Surfaces for Protein Adsorption and Cell Adhesion Regulation. *Colloids Surf., B* **2010**, *79*, 452−459.
(50) Cooper, J. A. Effects of Cytochalasin and Phalloidin on Actin. *J. Cell Biol.* **1987**, *105*, 1473−1478.
(51) Van Vaeck, L.; Adriaens, A.; Gijbels, R. Static Secondary Ion Mass Spectrometry (S-SIMS) Part 1: Methodology and Structural Interpretation. *Mass Spectrom. Rev.* **1999**, *18*, 1−47.
(52) Beamson, G.; Briggs, D. *High Resolution XPS of Organic Polymers. The Scienta ESCA300 Database.*; Wiley: Chichester, England, 1992.
(53) Zorn, G.; Liu, L.-H.; Árnadóttir, L.; Wang, H.; Gamble, L. J.; Castner, D. G.; Yan, M. X-ray Photoelectron Spectroscopy Investigation of the Nitrogen Species in Photoactive Perfluorophenylazide-Modified Surfaces. *J. Phys. Chem. C* **2014**, *118*, 376−383.
(54) Schmiers, H.; Friebel, J.; Streubel, P.; Hesse, R.; Köpsel, R. Change of Chemical Bonding of Nitrogen of Polymeric *N*-

Heterocyclic Compounds During Pyrolysis. *Carbon* **1999**, *37*, 1965−1978.
(55) Gilmore, I. S.; Seah, M. P.; Johnstone, J. E. Quantification Issues in ToF-SIMS and AFM Co-Analysis in Two-Phase Systems, Exampled by a Polymer Blend. *Surf. Interface Anal.* **2003**, *35*, 888−896.
(56) Lee, J. L. S.; Gilmore, I. S.; Seah, M. P. Quantification and Methodology Issues in Multivariate Analysis of ToF-SIMS Data for Mixed Organic Systems. *Surf. Interface Anal.* **2008**, *40*, 1−14.
(57) Venkataraman, N. V.; Pei, J.; Cremmel, C. V. M; Rossi, A.; Spencer, N. D. Template-Stripped, Ultraflat Gold Surfaces with Coplanar, Embedded Titanium Micropatterns. *Langmuir* **2013**, *29*, 9935−9943.
(58) Schneider, C. A.; Rasband, W. S.; Eliceiri, K. W. NIH Image to ImageJ: 25 Years of Image Analysis. *Nat. Methods* **2012**, *9*, 671−675.
(59) Curtis, A.; Forrester, J. V. The Competitive Effects of Serum-Proteins on Cell-Adhesion. *J. Cell Sci.* **1984**, *71*, 17−35.
(60) Steele, J. G.; Dalton, B.; Johnson, G.; Underwood, P. A. Polystyrene Chemistry Affects Vitronectin Activity: An Explanation for Cell Attachment to Tissue Culture Polystyrene but Not to Unmodified Polystyrene. *J. Biomed. Mater. Res.* **1993**, *27*, 927−940.
(61) Grinnell, F.; Feld, M. K. Fibronectin Adsorption on Hydrophilic and Hydrophobic Surfaces Detected by Antibody-Binding and Analyzed during Cell-Adhesion in Serum-Containing Medium. *J. Biol. Chem.* **1982**, *257*, 4888−4893.
(62) Geiger, B. 130K Protein From Chicken Gizzard—Its Localization at the Termini of Microfilament Bundles in Cultured Chicken-Cells. *Cell* **1979**, *18*, 193−205.
(63) Goldmann, W. H.; Ingber, D. E. Intact Vinculin Protein Is Required for Control of Cell Shape, Cell Mechanics, and Rac-Dependent Lamellipodia Formation. *Biochem. Biophys. Res. Commun.* **2002**, *290*, 749−755.
(64) Jönsson, U.; Ivarsson, B.; Lundstrom, I.; Berghem, L. Adsorption Behavior of Fibronectin on Well-Characterized Silica Surfaces. *J. Colloid Interface Sci.* **1982**, *90*, 148−163.
(65) Avnur, Z.; Geiger, B. The Removal of Extracellular Fibronectin from Areas of Cell-Substrate Contact. *Cell* **1981**, *25*, 121−132.
(66) Haynes, C. A.; Norde, W. Globular Proteins at Solid/Liquid Interfaces. *Colloids Surf., B* **1994**, *2*, 517−566.
(67) Garcia, A. J.; Vega, M. D.; Boettiger, D. Modulation of Cell Proliferation and Differentiation through Substrate-Dependent Changes in Fibronectin Conformation. *Mol. Biol. Cell* **1999**, *10*, 785−798.
(68) Underwood, P. A.; Steele, J. G.; Dalton, B. A. Effects of Polystyrene Surface Chemistry on the Biological Activity of Solid Phase Fibronectin and Vitronectin, Analysed with Monoclonal Antibodies. *J. Cell Sci.* **1993**, *104* (Pt 3), 793−803.
(69) Grinnell, F.; Feld, M. K. Adsorption Characteristics of Plasma Fibronectin in Relationship to Biological-Activity. *J. Biomed. Mater. Res.* **1981**, *15*, 363−381.
(70) Michael, K. E.; Vernekar, V. N.; Keselowsky, B. G.; Meredith, J. C.; Latour, R. A.; García, A. J. Adsorption-Induced Conformational Changes in Fibronectin Due to Interactions with Well-Defined Surface Chemistries. *Langmuir* **2003**, *19*, 8033−8040.
(71) Bergkvist, M.; Carlsson, J.; Oscarsson, S. Surface-Dependent Conformations of Human Plasma Fibronectin Adsorbed to Silica, Mica, and Hydrophobic Surfaces, Studied with Use of Atomic Force Microscopy. *J. Biomed. Mater. Res., Part A* **2003**, *64*, 349−356.
(72) Pompe, T.; Markowski, M.; Werner, C. Modulated Fibronectin Anchorage at Polymer Substrates Controls Angiogenesis. *Tissue Eng.* **2004**, *10*, 841−848.
(73) Ernst, O.; Lieske, A.; Holländer, A.; Lankenau, A.; Duschl, C. Tuning of Thermo-Responsive Self-Assembly Monolayers on Gold for Cell-Type-Specific Control of Adhesion. *Langmuir* **2008**, *24*, 10259−10264.
(74) Scheutjens, J. M. H. M.; Fleer, G. J. Statistical-Theory of the Adsorption of Interacting Chain Molecules. 1. Partition-Function, Segment Density Distribution, and Adsorption-Isotherms. *J. Phys. Chem.* **1979**, *83*, 1619−1635.